X-DoF

Automatic Degree-of-Freedom Subset Selection for Inverse Blocked Force Characterization

Bofinger, Philipp E.; Boelens, Jelle; Klaassen, Steven W.B.; De Klerk, Dennis

DOI
10.1115/1.4067081

Publication date
2025

Document Version
Final published version

Published in
Journal of Vibration and Acoustics

Citation (APA)
Bofinger, P. E., Boelens, J., Klaassen, S. W. B., & De Klerk, D. (2025). X-DoF: Automatic Degree-of-Freedom Subset Selection for Inverse Blocked Force Characterization. *Journal of Vibration and Acoustics*, *147*(1), Article 011002. https://doi.org/10.1115/1.4067081

ASME Journal of Vibration and Acoustics
Online journal at:
https://asmedigitalcollection.asme.org/vibrationacoustics

Philipp E. Bofinger[1]
VIBES.technology,
Löwengrube 12, München,
Oberbayern 80333, Germany
e-mail: pbofinger@vibestechnology.com

Jelle Boelens
VIBES.technology,
Burgwal 8a,
Delft, South Holland 2611 GJ, Netherlands
e-mail: jboelens@vibestechnology.com

Steven W. B. Klaassen
VIBES.technology,
Burgwal 8a,
Delft, South Holland 2611 GJ, Netherlands
e-mail: sklaassen@vibestechnology.com

Dennis de Klerk
Department of Precision and Microsystems
Engineering (PME), TU Delft,
Mekelweg 2,
Delft, South Holland 2628 CD, Netherlands;
VIBES.technology,
Burgwal 8a,
Delft, South Holland 2611 GJ, Netherlands
e-mail: ddeklerk@vibestechnology.com

X-DoF: Automatic Degree-of-Freedom Subset Selection for Inverse Blocked Force Characterization

Selecting the proper set of degrees-of-freedom (DoFs) is essential in inverse blocked force calculation. Including too many degrees-of-freedom in the computation can lead to overfitting, resulting in inaccurate force estimations and poor prediction quality. The discrepancy arises from errors within the dataset, such as measurement noise or other artifacts. This article presents a solution to the overfitting problem, introducing the X-DoF procedure to automatically identify the relevant subset of blocked force degrees-of-freedom. Its effectiveness is showed through numerical and experimental validation and compared against regularization techniques. [DOI: 10.1115/1.4067081]

Keywords: active vibration and noise control, dynamics, structural acoustics, system identification

1 Introduction

Component-based transfer path analysis (TPA) is an approach that uses blocked forces to simulate the vibration levels in new or modified products even before a prototype has been assembled. Blocked forces are the forces that one would obtain if the active component is measured against a rigid boundary [1], and hence, it is denoted as "blocked forces." They have gained popularity in TPA over the last few years because they are characteristic of only an active component such as an electric motor or compressor. Blocked forces can predict the responses on any receiving structure, like an electric vehicle. Predictions are computed by multiplying the blocked forces with the corresponding assembly's frequency response function (FRF) matrix.

In practice, it can be challenging to guarantee a rigid boundary condition in measurements, so the in situ method has been developed [2]. This method allows inversely calculating blocked forces in fully assembled structures, such as test benches or vehicles, with nonrigid boundary conditions. The in situ blocked force method has gained popularity in recent years and was standardized in ISO 20270:2019.

Although the in situ approach works well from a theoretical perspective, in real-life applications, the engineer is often faced with the problem of choosing the correct interface model. The predictive quality suffers from too few and too many degrees-of-freedom (DoFs) at the interface.

The dynamics are not sufficiently described if too few or incorrect DoF are selected. Alternatively, choosing too many DoFs can cause the so-called overfitting. Overfitting often manifests itself in too high or nonphysical force estimates. A manual deselection of DoF can be performed to reduce or circumvent overfitting. But this process of trial and error quickly becomes a tedious task as the number of possible subsets rises exponentially by 2^m with m being the total number of blocked force DoF. In addition, the blocked force computation is performed for each frequency separately, and one often finds that different DoFs are active in various frequency ranges of interest.

This article proposes an approach, denoted X-DoF, to automatically select the relevant subset of blocked force DoF. X-DoF allows gaining insight into the interface dynamics at play and mitigates the risk of overfitting. The proposed procedure increases accuracy and does not require additional user input or validation measurements. This makes the in situ method efficient and less prone to errors caused by engineering practices, understanding, and taste. As such, in situ blocked force estimates using X-DoF result in a considerable gain in time efficiency and robustness. In addition, one might add more DoF to the interface without the risk of overfitting measurement noise.

The subsequent sections first provide the theory of the in situ blocked force method in the realm of component TPA. Fitting a polynomial equation is used to illustrate the effects of overfitting and regularization, which is common practice in TPA. The article

[1]Corresponding author.

Contributed by the Technical Committee on Vibration and Sound of ASME for publication in the Journal of Vibration and Acoustics. Manuscript received July 15, 2024; final manuscript received October 30, 2024; published online November 26, 2024. Assoc. Editor: Julien Meaud.

continues with an overview of the X-DoF procedure and concludes with real-life examples.

2 Theory of the Component Transfer Path Analysis Method

Component-based TPA comprises several techniques to characterize vibration sources with equivalent or often called blocked forces. The methods study the vibration propagation in the product up to the relevant passive side responses like, for vehicle development, microphones at the driver's ears. The basic outline of the methodology is presented here. For a more extensive explanation, the authors refer the reader to Ref. [1] or alternatively, including use cases, in Refs. [3,4].

Figure 1 shows an arbitrary system consisting of two subsystems. Subsystem A is denoted the "active component" as it contains an often immeasurable vibration source. Subsystem B is denoted the "passive component" as it does not contain vibration sources and merely experiences the vibration introduced by the active component through their interfaces.

The derivation of the component-based TPA method starts with the equations of motion of the assembled system FRF, shown in Fig. 1, in a block diagonal form:

$$\begin{bmatrix} \mathbf{u}_1^A \\ \mathbf{u}_2^A \\ \mathbf{u}_2^B \\ \mathbf{u}_3^B \end{bmatrix} = \begin{bmatrix} \mathbf{Y}_{11}^A & \mathbf{Y}_{12}^A & . & . \\ \mathbf{Y}_{21}^A & \mathbf{Y}_{22}^A & . & . \\ . & . & \mathbf{Y}_{22}^B & \mathbf{Y}_{23}^B \\ . & . & \mathbf{Y}_{32}^B & \mathbf{Y}_{33}^B \end{bmatrix} \left(\begin{bmatrix} \mathbf{f}_1^A \\ . \\ . \\ . \end{bmatrix} + \begin{bmatrix} . \\ \mathbf{g}_2^A \\ \mathbf{g}_2^B \\ . \end{bmatrix} \right) \tag{1}$$

where $\mathbf{g}_2^A$ and $\mathbf{g}_2^B$ are vectors with the interface forces acting between the active subsystem A (denoted with a superscript) and passive subsystem B. Capital $\mathbf{Y}$ denotes receptance (e.g., FRF) matrices, $\mathbf{u}$ denotes displacements, and $\mathbf{f}$ denotes externally applied forces. Subscripts 1–3 denote different collections of DoF for the respective vector and matrix entities:

- 1—Internal: All DoFs on or in the active component that apply (most often) immeasurable forces.
- 2—Interface: All DoFs at the interface between the active and passive sides.
- 3—Target: The DoF collection on the passive side of which the responses due to the active component excitation are of interest.

Let us first determine the system response due to the internal excitation force and then derive the alternative formulation using blocked forces. To determine the system response, we combine lines 2 and 3 from equation (1) to express displacement compatibility ($\mathbf{u}_2^A = \mathbf{u}_2^B$), yielding:

$$\mathbf{Y}_{21}^A \mathbf{f}_1^A + \mathbf{Y}_{22}^A \mathbf{g}_2^A = \mathbf{Y}_{22}^B \mathbf{g}_2^B \tag{2}$$

By substituting the force equilibrium ($\mathbf{g}_2^A = -\mathbf{g}_2^B$), for the coupled system, one finds:

$$\mathbf{g}_2^B = (\mathbf{Y}_{22}^A + \mathbf{Y}_{22}^B)^{-1} \mathbf{Y}_{21}^A \mathbf{f}_1^A \tag{3}$$

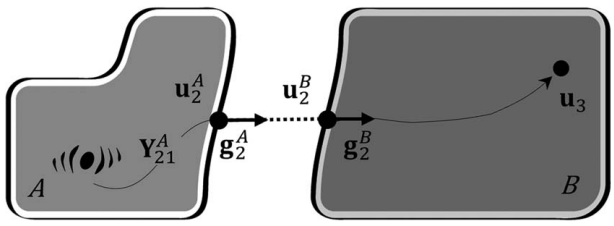

Fig. 1 Source identification problem with the active component *A* and the passive component *B*

Combining with line 4 from Eq. (1), we find the passive side responses as a function of the interface forces[2] or internal forces from the active subsystem as follows:

$$\mathbf{u}_3^B = \mathbf{Y}_{32}^B \mathbf{g}_2^B = [\mathbf{Y}_{32}^B (\mathbf{Y}_{22}^A + \mathbf{Y}_{22}^B)^{-1} \mathbf{Y}_{21}^A] \mathbf{f}_1^A \tag{4}$$

It can be verified [1] that the expression within the brackets [..] is equivalent to $\mathbf{Y}_{31}^{AB}$, and hence, Eq. (4) can also be written as follows:

$$\mathbf{u}_3^B = \mathbf{Y}_{31}^{AB} \mathbf{f}_1^A \tag{5}$$

The excitation force $\mathbf{f}_1$ is typically immeasurable and the interface force $\mathbf{g}_2^B$ is influenced, see Eq. (3), by the passive side's dynamics. Equation (5), therefore, is not a proper way to characterize the source independent from its passive side. To derive an independent source characterization, let us therefore focus on finding externally applied forces in the form:

$$\mathbf{u}_3^B = \mathbf{Y}_{32}^{AB} \mathbf{f}_2 \tag{6}$$

where $\mathbf{f}_2$ represents a set of blocked forces, yet to be determined, that yield responses $\mathbf{u}_3^B$ that are equivalent to the original excitation by the internal force $\mathbf{f}_1^A$. Analog to the simplification of Eqs. (4) and (5), one can rewrite Eq. (6) in subsystem dynamics as follows:

$$\mathbf{u}_3^B = \mathbf{Y}_{32}^B \left(\mathbf{Y}_{22}^A + \mathbf{Y}_{22}^B\right)^{-1} \mathbf{Y}_{22}^A \mathbf{f}_2 \tag{7}$$

By combining Eqs. (7) and (4), one finds blocked forces acting on the component interface as follows:

$$\mathbf{f}_2 = \left(\mathbf{Y}_{22}^A\right)^{-1} \mathbf{Y}_{21}^A \mathbf{f}_1^A \tag{8}$$

Note that the derivation of $\mathbf{f}_2$ is independent of the passive side's dynamics and, hence, is determined by the active system's dynamics only. As $\mathbf{f}_1^A$ is, however, difficult or impossible to measure in practice, Eq. (8) is of little practical value so far. Combining Eq. (8) with line 2 from Eq. (1), after premultiplication with $\left(\mathbf{Y}_{22}^A\right)^{-1}$, one finds a much more practical formulation:

$$\mathbf{f}_2 = \left(\mathbf{Y}_{22}^A\right)^{-1} \mathbf{u}_2^A + \mathbf{g}_2^B \tag{9}$$

Equation (9) shows that the blocked forces, replacing the internal forces $\mathbf{f}_1^A$, can be derived directly from a measurement of the interface forces and displacements in the assembled configuration. Based on Eq. (9), one can distinguish two special cases:

- $\mathbf{g}_2^B = 0$. In this case, as no interface forces act between the active and passive side, the active source is dismounted from the passive side. The blocked forces are found from the interface motion and the properties of the active component only. This special case, also referred to as the free velocity method, is described in ISO 9611.
- $\mathbf{u}_2^A = 0$. This case corresponds to a rigid boundary condition as the interface does not experience any motion. The measured interface forces are equal to the blocked forces themselves now, i.e., forces measured at the interface while the active component is fixed on a rigid test bench.

Equation (9) still requires impractical measurement of interface forces. A further simplification is possible by substitution of Eq. (1), line 3, into Eq. (9):

$$\mathbf{f}_2 = \left(\mathbf{Y}_{22}^A\right)^{-1} \mathbf{u}_2^A + \left(\mathbf{Y}_{22}^B\right)^{-1} \mathbf{u}_2^B \tag{10}$$

[2]Classical TPA methods like the direct force, mount stiffness, and matrix inverse method use Eq. (4) ($\mathbf{u}_3^B = \mathbf{Y}_{32}^B \mathbf{g}_2^B$) directly to characterize the active component excitation using interface force $\mathbf{g}_2^B$ and the assembled system response $\mathbf{u}_3^B$ from the passive subsystem FRF. In practice, it requires dismounting the active component from the assembly.

which, as dynamic stiffness matrices may be simply added, is equivalent to:

$$\mathbf{f}_2 = \left(\mathbf{Y}_{22}^{AB}\right)^{-1}\mathbf{u}_2 \tag{11}$$

Equation (11) shows a quite remarkable result, namely:

> *The blocked forces, characterizing the active component's excitation independent from the passive side's dynamics, can be determined in situ directly and do not require dismounting the active component from the assembly or measurement on a rigid bench.*

FRF measurements on the interface itself are, in practice, also difficult to achieve. Therefore, the force DoFs from an impact hammer test are transformed to obtain a description at the interface, for example, using the virtual point transformation [5]. Instead of using response DoF at the interface, one can estimate $\mathbf{f}_2$ using a different set of indicator DoF on the passive side. See Fig. 2 where a collection of DoF by set number 4 is introduced.

Measuring responses for set 4 yields a characterization FRF matrix $\mathbf{Y}_{42}^{AB}$ that is preferably overdetermined [6,7]. Thereafter, one can estimate the blocked forces from an operational measurement, analogous to the classic matrix inverse method [1]:

$$\mathbf{f}_2 = \left(\mathbf{Y}_{42}^{AB}\right)^{+}\mathbf{u}_4 \tag{12}$$

Equation (12) describes the in situ blocked force characterization, which was standardized in ISO20270:2019. Notice, however, compared to the classic matrix inverse method, that the FRF data are determined on the assembled system *AB* and not on the passive side *B* only. Furthermore, $\mathbf{f}_2$ represents a true source characterization of the active component, independent of the passive side it is connected to.

With the in situ derivation completed, the authors would like to end with some important notes on the theoretical basis:

- The method is based on the assumption of linearity and time invariance. Actual machines might not behave this way. In those cases, one should try to measure the system in its operating state and perform analysis, including the additional nonlinear parameters.
- One assumes that set 4 can replace set 2 when utilizing Eq. (12). Effectively, one needs to determine if set 4 can truly observe the effect of set 2 correctly and sufficiently. Wrong choices will lead to erroneous force predictions.
- Equation (12) does not depend on any particular interface description. However, the results depend on modeling choices for the interface description. In practice, the engineer is confronted with the question of how many and which DoF is needed to describe the interface. The in situ method can easily suffer from underfitting or overfitting if poor choices are made.

3 Quality Assessment of Blocked Force Estimates

To determine if blocked forces suffer from underfitting or overfitting, we introduce three levels of analysis.

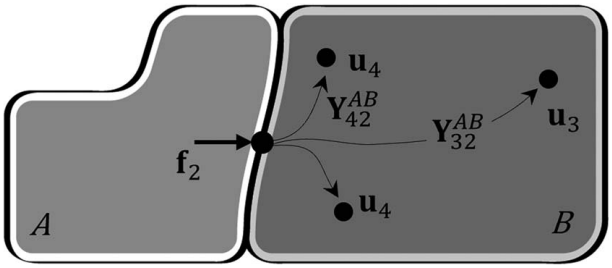

Fig. 2 In situ blocked forces calculated from indicator responses $\mathbf{u}_4$ and the characterization FRF $\mathbf{Y}_{42}^{AB}$

3.1 Indicator Validation. An indicator validation can reveal if the blocked forces suffer from underfitting and is defined as follows:

$$\mathbf{u}_4 \overset{?}{=} \mathbf{Y}_{42}^{AB}\left(\mathbf{Y}_{42}^{AB}\right)^{+}\mathbf{u}_4 \tag{13}$$

Blocked forces are computed according to the in situ method with a set of chosen indicator sensors $\mathbf{u}_4$ to thereafter determine if the force estimate can predict the measured responses of the indicator sensors. This is analogous to determine the residual in least-squares methods. By evaluating the residual at and from the chosen indicator sensors, one finds if the forces can control them. If this yields unsatisfactory fits, one is sure to either have inconsistent models, chosen too few BF DoF, or the indicator sensors suffer from noise issues.

3.2 Onboard Validation. The second method to determine if one suffers from either overfitting or underfitting is the so-called onboard validation, which is documented as a mandatory check in ISO 20270:2019. In contrast to indicator validation, the residual is now evaluated on (different) independent validation sensors $\mathbf{u}_3$. These validation sensors are part of the same test assembly to determine the blocked forces, but not part of their computation:

$$\mathbf{u}_3 \overset{?}{=} \mathbf{Y}_{32}^{AB}\left(\mathbf{Y}_{42}^{AB}\right)^{+}\mathbf{u}_4 \tag{14}$$

If a large discrepancy is found, it may be due to underfitting or overfitting.[3] The engineer should reevaluate the setup, the selected forces, and the indicator sensors. However, we noticed that an onboard validation can be insufficiently sensitive to observe overfitting. This can be the case if the dynamics at the validation sensors are similar to the dynamics at the indicators, e.g., $\mathbf{Y}_{42}^{AB} \approx \mathbf{Y}_{32}^{AB}$, $\mathbf{u}_4 \approx \mathbf{u}_3$. In this case, an onboard validation only displays underfitting, compare Eq. (13).

3.3 Transfer Validation. Although requiring another test setup and hence effort, a so-called transfer validation can serve as an improved method to determine overfitting. Here, one determines the blocked forces, for example, on a component test bench. Thereafter, these forces are applied to a different setup, where the active component is, for example, fitted to the vehicle or a different test-bench design. By combining the two FRF and operational tests, the transfer validation is computed as follows:

$$\mathbf{u}_3^{AR} \overset{?}{=} \mathbf{Y}_{32}^{AR}\left(\mathbf{Y}_{42}^{AB}\right)^{+}\mathbf{u}_4^{AB} \tag{15}$$

Here, *AB* denotes the original measurement configuration and index *AR* denotes the modified setup or, better, the active component mounted to a completely different passive side. Either way, the dynamics in both configurations need to differ considerably, i.e., $\mathbf{Y}_{42}^{AB} \neq \mathbf{Y}_{32}^{AR}$. Now, one can answer the question of whether the blocked forces found are a proper generalization and describe the source independent of its receiving structure. If the measured validation responses are the same as the computed ones in the original setup, the blocked forces are proper and unique. Mathematically, one can now verify the predictive quality of the blocked forces outside of their "training environment."

While the transfer validation is a good way to confirm the correctness of the forces, the process is quite tedious. In general, the desire exists to get robust blocked force estimates on the original test-bench itself and deal with the overfitting issue directly. For that reason, this article introduces the X-DoF approach. The next two sections first illustrate the overfitting issue on a least-squares fit of

[3] An onboard validation of a response $\mathbf{u}$ due to an artificial excitation is less likely to overfit noise because artificial excitations generally result in a good signal-to-noise ratio. If the response is normalized to the input force, this test is closely related to the interface completeness criterion (ICC) [8], which can be used to quantify underfitting.

a polynomial function (see Sec. 4) to solve the issue thereafter using the X-DoF procedure (see Sec. 5).

4 The General Problem With the Current State of the Art

While inverse problems in general and hence the in situ blocked force characterization methods offer flexibility in the modeling choices, this flexibility becomes a downside when too few, or too many DoF are included.

4.1 Overfitting Issue in Regression. An overfitted model consists of more parameters than can be justified by the data [9]. This effect can be visualized by a least-squares fit of a polynomial function with an increasing amount of DoF and added noise [10]. Figure 3 shows the function $y = 1 + x + x^2$ used in this article.

The data in the range of x from –1 to 0.5 is used to fit the models. The values between 0.5 and 3 validate the models' predictions on unseen data. We generate a sample set of this function with 1% of Gaussian noise to model inconsistencies of measurements. This can be written as a system of equations:

$$\begin{bmatrix} 1 & x_1 & x_1^2 & \cdots & x_1^n \\ \vdots & \vdots & \vdots & \cdots & \vdots \\ 1 & x_r & x_r^2 & \cdots & x_r^n \end{bmatrix} \begin{bmatrix} c_0 \\ \vdots \\ c_n \end{bmatrix} = \begin{bmatrix} y_1 \\ \vdots \\ y_r \end{bmatrix} \tag{16}$$

with $\mathbf{x}_i^j$ being the polynomial function matrix with samples $i = 1$ to r and polynomial degree $j = 0$ to n. $\mathbf{y}$ is the data at r samples with added noise. Vector elements c_0 to c_n represent the unknown coefficients. Ideally, one should find a value of one for c_0 to c_2 and zero for any higher-order coefficients c_3 to c_n. Their least-squares solution is computed via the pseudo inverse, analogous to the in situ method (12):

$$\mathbf{c} = (\mathbf{X}_{\text{training}})^{+}\mathbf{y}_{\text{training}} \tag{17}$$

Then, the polynomial matrix containing all r samples is multiplied with the estimated coefficients to obtain predictions in the training and validation regions.

$$\mathbf{X}\mathbf{c} = \mathbf{y}_{\text{predicted}} \tag{18}$$

This procedure is repeated for an increasing amount of maximum polynomial degree n up to 5.

As can be observed in Fig. 4, the solution with the correct DoF amount (polynomial degree 2 including a constant, a linear, and a quadratic term) shows the best predictions of the unseen data in the validation interval. Models with fewer *and* more DoF show reduced prediction quality, illustrating the effect of both underfitting and overfitting, respectively.

It is interesting to note that the residual within the training set actually keeps dropping more and more with increasing DoF, see Fig. 5. Models of higher orders yield lower residuals due to the

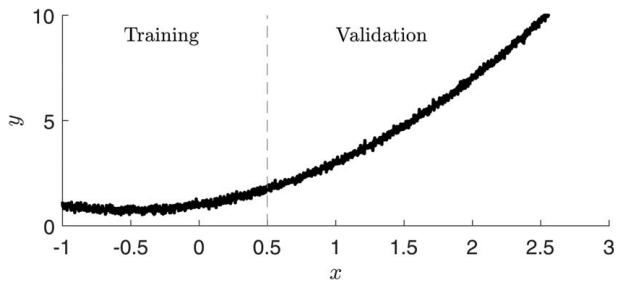

Fig. 3 The quadratic function with added Gaussian noise is split into a training set and a validation set

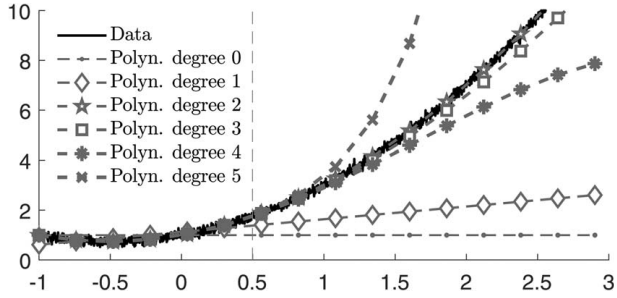

Fig. 4 Least-squares regression of the data and prediction with increasing polynomial degree

approximation of noise on the fitted interval compared to the true model with polynomial degree 2.

Hence as illustrated in this example, overfitted models do yield good predictions on the training region and fit the noise present very well. However, the models do not transfer well to another validation measurement and, therefore, have a lower predictive quality.

Besides the reduced prediction quality, performing the least-squares regression with irrelevant DoF can negatively influence the solution's robustness to noise. To demonstrate this effect, the regression is repeated 200 times with randomly added Gaussian noise of 1 %. The calculated coefficients are displayed in Fig. 6. An x marks the true value, and the least squares estimate has a box centerline representing the median value and the bottom and top box edges indicating the 25th and 75th percentiles. The black lines above and below the box represent the maximum and minimum data values, respectively, that is not an outlier.

One finds by modeling the function correctly (constant, linear, and quadratic terms) that the values match the true values very well, i.e., on average, one finds the proper solution (Fig. 6, left side).

The coefficients of the regression with 6 DoF are shown on the right side of Fig. 6. As previously observed, the predictive quality of this overfitted model was quite poor. Here, we see that the solution is furthermore also very sensitive to only 1 % noise, as

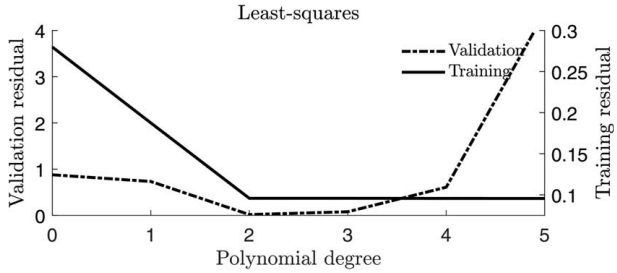

Fig. 5 Least-squares residual inside and outside the training bounds with increasing DoF amount

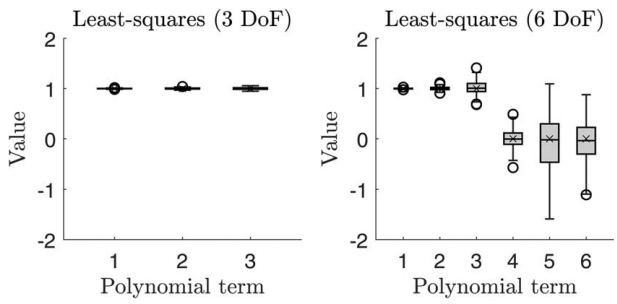

Fig. 6 Least-squares solutions in the case of modeling the correct DoF (left) and too many DoF (right)

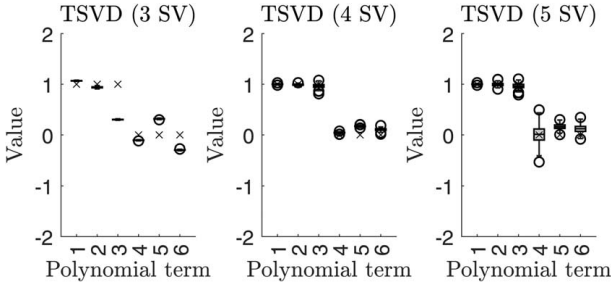

Fig. 7 Truncated SVD solutions when modeled with three (left), four (middle), and five (right) singular values

illustrated by the high standard deviations and outer bands. The solution of the relevant DoF 1–3 shows greater deviations compared to the 3-DoF regression, and furthermore, nonzero values are fitted in irrelevant terms 4–6.

In the realm of component-based TPA, this means that noise on indicator sensors can lead to overfitted blocked forces when the interface contains irrelevant DoF. This compromises the accuracy and predictive quality of blocked forces. Only a model with the correct set of blocked force DoF will accurately describe the measured dynamics without overfitting indicator sensor noise or other inconsistencies.

4.2 Improving the Robustness to Noise With Matrix Regularization. A common practice in inverse problems with test-based data is to perform a singular value decomposition (SVD) on the matrix to be inverted, with the idea of reducing the effect of noise or small artifacts in the data [11,12]. In the remainder of this section, we illustrate that this method's effect is only limited.

Based on the singular values σ, the condition number κ can be calculated by the ratio of the largest to the smallest singular value:

$$\kappa = \frac{\sigma_{\max}}{\sigma_{\min}} \tag{19}$$

The estimated solution's signal-to-noise ratio decreases proportional to the condition number of the matrix [10]. For this reason, large condition numbers can amplify measurement noise.

One way to improve the conditioning number is to truncate the singular value decomposition (TSVD) [13]. It is important to note that lowering the number of singular values in the model estimation actually reduces the DoF space, i.e., the freedom from each DoF to approximate the measurements.[4] Every singular value removed constrains the DoF from one another such that they may only move in certain combinations that capture the most variance, but not necessarily the relevant DoF.

To illustrate the effect, Fig. 7 shows the model fit and spread when removing one to three singular values from the 6 DoF polynomial function fit. The following can be observed:

- The model estimates become more consistent with less deviation and hence a lower standard deviation. Regularization minimizes the effect of the noise.
- However, the median model estimates actually do start to differ more and more from the true values that should be found while decreasing the amount of singular values in the model. Hence, while reducing the influence of noise, one introduces bias errors.
- Once reduced to the right amount of DoF (i.e., three singular values), the model fit is rather off and bias errors prevail.

This trade-off shows that while reducing the model variability can be achieved with a truncated model, the likelihood of converging to the true solution actually decreases when using a truncated SVD.

A more sophisticated way to improve the conditioning number is the use of Tikhonov regularization [15], which modifies the singular values according to the following equation:

$$\sigma_i^{\text{tik}} = \frac{\sigma_i}{\sigma_i^2 + \lambda} \tag{20}$$

with λ being the regularization parameter. Applying this technique yields the model fit shown in Fig. 8. While improving perhaps somewhat, it is clear that Tikhonov regularization also doesn't yield a proper model.

In conclusion, this section illustrates that matrix regularization via Tikhonov and TSVD can reduce the influence of measurement noise but at the cost of bias. For in situ blocked force calculation, these methods are unlikely to yield better solutions compared to modeling the system with the correct set of DoF.

5 X-DoF Procedure for Selecting the Relevant Subset of Degree-of-Freedom

To reduce the problem of overfitting in blocked force characterization, one needs to select the right DoF subset of a typically over-modeled interface. X-DoF is a procedure that does so by utilizing a combination of sparse regression techniques and model selection criteria. Note that this approach is not limited to the inverse blocked force characterization and could be applied to other inverse problems.

5.1 Best Subset Selection. Best subset selection aims to obtain models from a subset of available DoF to describe the measurements. We assume that the full characterization FRF $\mathbf{Y}_{42}$ has at least the relevant DoF to describe the measurements $\mathbf{u}_4$ sufficiently. One can validate this assumption by applying the methods in Sec. 3. For each subset size j from 0 to the total number of m DoF, the subset is identified that minimizes the least-squares residual

$$\mathbf{f}_{2,j} = \arg\min_{\mathbf{f}_2} \|\mathbf{u}_4 - \mathbf{Y}_{42}\mathbf{f}_2\|_2 \qquad \text{s.t.} \quad \|\mathbf{f}_2\|_0 \leq j \tag{21}$$

with the zero-norm $\|\mathbf{f}_2\|_0$ counting the number of nonzero elements of the force vector. One may solve for all possible subsets and then select the ones that minimize the residual at each j. However, this is not advisable for a large number of DoF because the number of possible subsets rises exponentially by 2^m. To improve the computational cost, one could leverage optimization methods, stepwise selection techniques, or the least absolute shrinkage and selection operator [16,17]. Some of these methods are guaranteed to be optimal and computationally expensive, and others are only asymptotically optimal at a lower cost.

The results in this work are obtained by performing a setpwise selection with orthogonal least squares (OLS) [18]. An implementation of OLS can be found in Ref. [19]. At each iteration, a

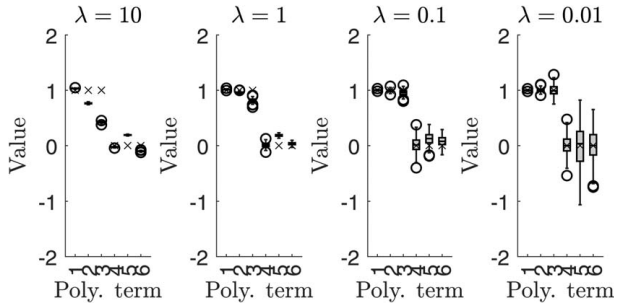

Fig. 8 Solutions with Tikhonov regularization for a varying regularization parameter λ

[4]Removing singular values also reduces the total energy of an FRF matrix [14].

single DoF i is added to an active set $\mathcal{A}$ based on the following heuristic. Of all DoF not in the active set, the DoF that minimizes the least-squares residual is selected:

$$\arg\min_{i \notin \mathcal{A}} \|\mathbf{u}_4 - \mathbf{Y}_{42}^{\mathcal{A} \cup i} \mathbf{f}_2\|_2 \tag{22}$$

For a system with $m = 24$ DoF, an exhaustive search requires solving $2^m = 16777216$ systems of equations. OLS reduces this number to $m + (m-1) + +1 = 300$ evaluations. The best subset selection results in $m + 1$ candidate models $\mathbf{f}_{2,j}$. As a next step, the candidate solutions are scored against each other to select the best solution within these candidates.

5.2 Model Selection. The goal of the model selection step is to select the candidate model that achieves generalization to unseen data. In the polynomial example case, this would be selecting the model of polynomial degree 2 because this minimizes the residual on the validation data, compare Fig. 5. However, we believe that selecting the blocked force interface model based on splitting the data into training and validation can have several drawbacks:

- An onboard validation can not always observe overfitting, especially when the dynamics of the characterization and prediction FRF are similar, compare equation (14).
- The background noise of test benches often influences onboard validation sensors. In addition, these sensors can not always be included in measurement setups, e.g., in free-free conditions.
- Alternatively, one could split the indicator data $\mathbf{u}_4$ into a training and a validation set. However, this would require placing additional sensors to achieve sufficient overdetermination. Adding sensors is often challenging due to limited interface accessibility.

Instead, model selection criteria are applied, which estimate the validation error. They are based on the training error and are adjusted to account for overfitting. For the results in this work, the model is selected, which minimizes the Mallow's Cp statistic [20]:

$$\mathrm{C\,p}_j = \frac{\mathrm{RSS}_j}{\hat{\sigma}^2} - n + 2k \tag{23}$$

with n being the number of observations in the data, $k = \|\mathbf{f}_2\|_0 + 1$ being the number of independent variables, and RSS being the residual sum of squares:

$$\mathrm{RSS}_j = \|\mathbf{u}_4 - \mathbf{Y}_{42}\mathbf{f}_{2,j}\|_2^2 \tag{24}$$

and $\hat{\sigma}^2$ being an estimate for the variance of the error, which is often obtained from the full model containing all DoF as RSS_m/n. Alternative selection criteria include the corrected Akaike information criterion [21] or the Bayesian information criterion [22]. Note that these model selection criteria are limited to overdetermined systems of equations in which the RSS is generally nonzero.

5.3 Numerical Results. To validate the X-DoF procedure, the previous regression test is repeated. The polynomial terms of degree 5 are included in the regression. The X-DoF solution shows an improved prediction into the validation region when compared to the least-square solution or regularization, as shown in Fig. 9.

X-DoF reduces overfitting because the validation residual does not increase with irrelevant terms in the regression, see Fig. 10.

X-DoF yields an accurate identification of the correct terms, see Fig. 11. The robustness to noise also increases because sparsity improves the conditioning of the system. Solutions from X-DoF match the results obtained via least squares if modeled with the correct 3 DoF, compare Fig. 6. In other words, additional DoF can be included without the overfitting risk.

In summary, this section shows that X-DoF reduces overfitting and improves the solution's robustness to noise by selecting the correct subset of DoF. Solutions based on X-DoF are also more accurate and generalize better than those based on other methods, such as matrix inverse, TSVD, and Tikhonov regularization. The same benefits are expected for blocked forces calculated based on the X-DoF procedure. This is evaluated in the following section.

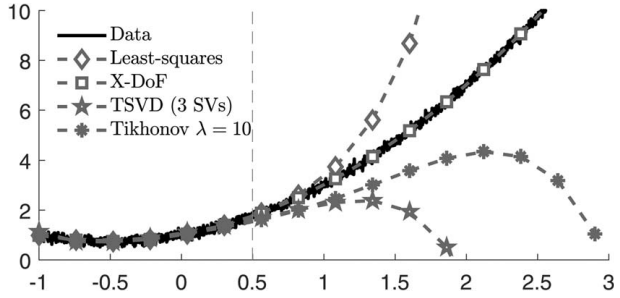

Fig. 9 Predictions of a least-squares, regularization, and X-DoF model, each with 6 polynomial DoF

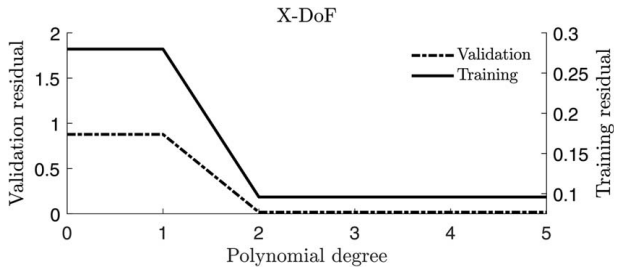

Fig. 10 X-DoF model residual inside and outside the training bounds with increasing DoF amount

6 Experimental Results

In this section, X-DoF is experimentally tested for the physicality of the calculated blocked forces and their predictive quality in onboard and transfer validations.

6.1 Blocked Force Degree-of-Freedom Selection. Our first experimental test's objective is to assess the selection of calculated blocked force DoF from a known input on a freely suspended electric power steering with two 6-DoF virtual points (VPs), see Fig. 12.

Blocked forces are calculated from the response due to excitation with an impact hammer (artificial excitation) scaled to 1 N. Figure 13 shows the artificial excitation pointed in the z-direction with an offset of 13 mm in the x-direction and 8 mm in the y-direction to the right virtual point.

Assuming local rigidity, a combination of a force in the z-direction with moments around x and y should be sufficient to

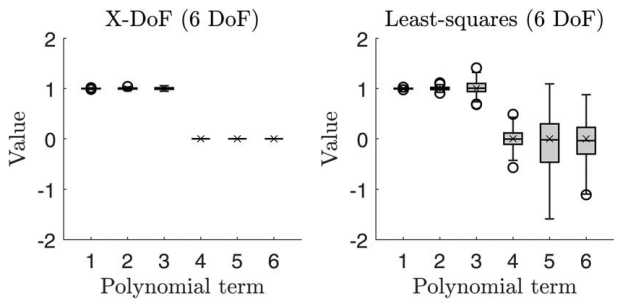

Fig. 11 X-DoF solutions (left) and the least-squares solutions (right) with irrelevant terms (4–6) included

Fig. 12 Electric power steering setup with a 6-DoF virtual point on the left and right sides

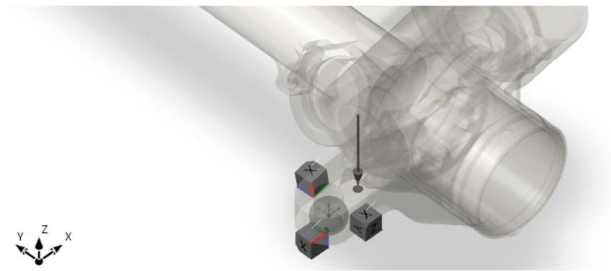

Fig. 13 Artificial excitation at the right virtual point in the *z*-direction with an offset in *x*- and *y*-directions

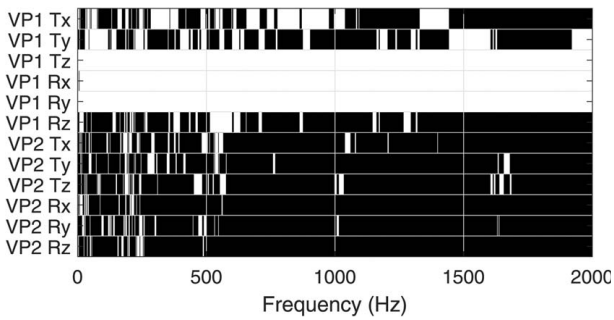

Fig. 14 Subset of active blocked force DoF selected by X-DoF. Inactive DoF are depicted in black.

block the interface for the artificial excitation. Modeling this with a total of 12 DoF could lead to overfitting. The active subset of blocked force DoF, automatically selected by X-DoF, is shown in Fig. 14.

X-DoF selects the subset of relevant DoF (Tz, Rx, and Ry) at the right virtual point. It is noteworthy that forces in Tx and Ty are also selected at some frequencies. Inconsistencies in the experiment might have caused this or if the artificial excitation was not performed perfectly in the *z*-direction.

Ideally, the magnitude of the translational z force is expected to be 1 N over the frequency range. In Fig. 15, the solution is depicted for X-DoF, matrix inverse, TSVD, and Tikhonov regularization.

The X-DoF and matrix inverse solutions are closest to the analytical solution of 1 N. The TSVD is performed with six singular values, a popular choice to model for rigid body behavior. A Tikhonov regularization is calculated with $\lambda = 0.001$. These regularization techniques yield translational forces that significantly deviate from the reference solution. The deviations can be explained through the bias introduced by both methods, compare Sec. 4.2.

To fulfill moment equilibrium, the moments should scale with 1 N times the distance of the artificial impact from the virtual point. The moments calculated based on X-DoF and the matrix inverse method match the reference given by 0.008 Nm in Rx and 0.013 Nm in Ry, see Fig. 16. TSVD and Tikhonov regularization show larger deviations.

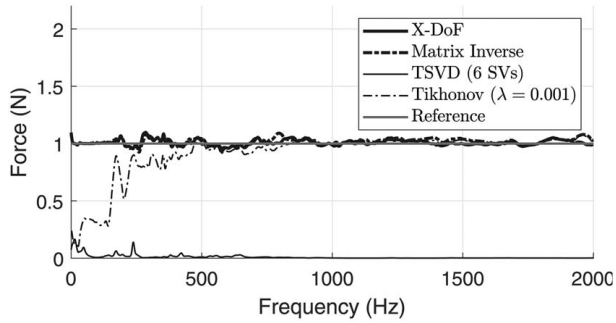

Fig. 15 Blocked force in Tz at the right VP

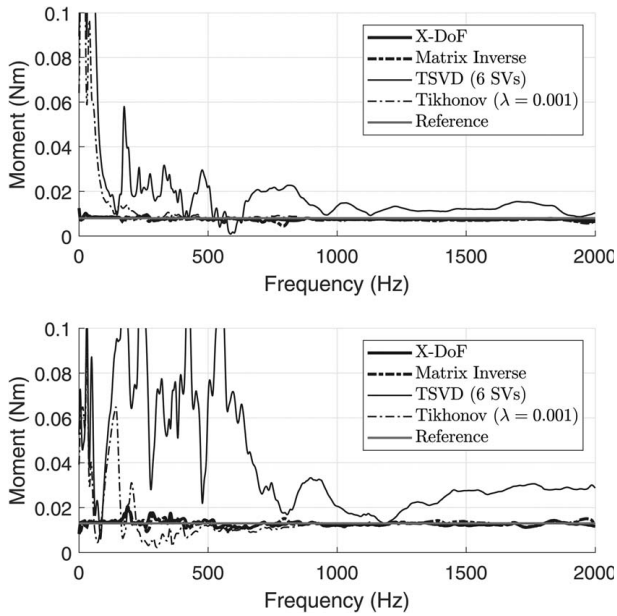

Fig. 16 Blocked moments Rx (top) and Ry (bottom) at the right VP

Overall, the blocked forces from the matrix inverse approach and X-DoF match well with the analytical solution. Although X-DoF selects a much smaller subset of forces, the results are similar to the full inverse using all 12 DoF. Similar solutions are expected because artificial excitations are less susceptible to overfitting due to their high signal-to-noise ratio. Nevertheless, X-DoF demonstrates its data-driven capabilities in selecting the correct subset of DoF. In addition, this experiment underlines that TSVD and Tikhonov regularization can result in deteriorated outcomes due to bias errors. This result should be further investigated to clarify the limitations of these methods in accurately determining blocked forces.

6.2 Blocked Force Predictions. The next step is to validate the predictive quality of blocked forces calculated using X-DoF on three active components from the automotive industry.

6.2.1 Electric Power Steering. The first example is an electric power steering (EPS). Unlike the previous case, the EPS is now mounted on a test-bench, and four virtual points are used to model the interface. See Fig. 17 for a representative setup.

Initially, an indicator validation is performed to check if the amount of chosen DoF is sufficient to model the measured responses, see Eq. (13) and Fig. 18.

Above 200 Hz, the indicator fit matches the measurement well. Therefore, four 6-DoF virtual points are sufficient to "interpolate" the data. Below 200 Hz, the fit yields unsatisfactory results. As

Fig. 17 Representative EPS setup with four VPs

this discrepancy is only found at lower frequencies, this indicates sensor noise issue, which is plausible due to a relatively rigid test bench design. This limits the applicability of the blocked forces to the region above 200 Hz. A way to improve this test bench for blocked force characterization would be to design it more flexibly.

Once the blocked forces have been computed, they are applied to the structure to predict the acceleration at validation sensors. The prediction is then compared with the actual measured signal obtained at these sensors, see Eq. (14) and Fig. 19. The predictions below 200 Hz should not be evaluated due to the noise issues previously mentioned. Above 200 Hz, the onboard validation calculated with X-DoF matches the measurement well. The prediction based on the matrix inverse method shows signs of overfitting. This indicates that all 24 interface-DoFs contain irrelevant DoF to model this steering excitation.

6.2.2 Electric Drive Unit. A second test is performed on an electric drive unit (EDU) mounted on a test bench, see Fig. 20.

The indicator validation in Fig. 21 shows a good match between the measured data and the model fit. Therefore, the chosen amount of DoF should contain a DoF subset to describe the measured EDU responses for this operational condition sufficiently.

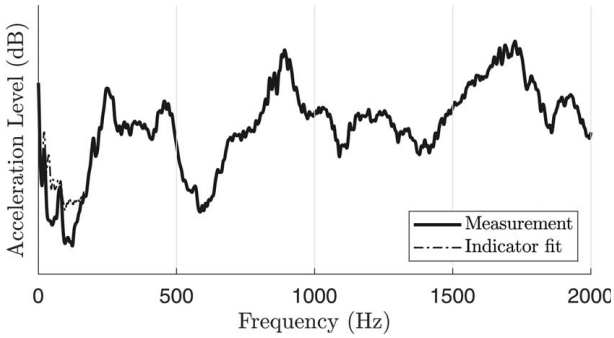

Fig. 18 Indicator validation revealing underfitting of the model below 200 Hz

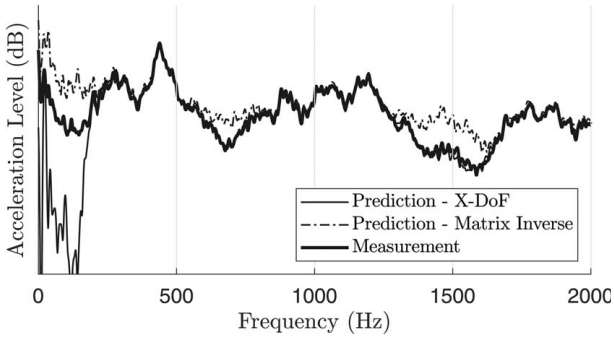

Fig. 19 Onboard validation indicating less overfitting with X-DoF compared to the matrix inverse

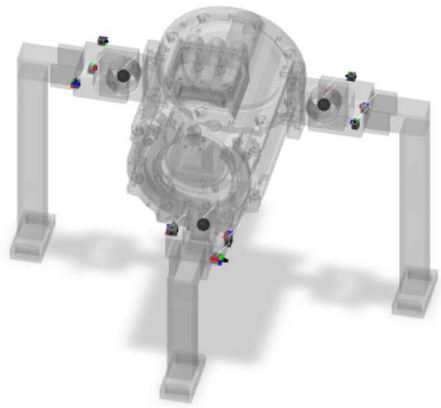

Fig. 20 Experimental test setup of an electric drive unit with three virtual points

In the onboard validation, the X-DoF solution predicts the closest to the reference, while the matrix inverse method deviates, compare Fig. 22. This indicates that the system is overmodeled with 18 DoF, and X-DoF successfully selects a proper subset.

The relevant interface description for this operating condition can be visualized from the active subset selected by X-DoF, compare Fig. 23.

Overall, fewer than the full set of 18 DoF are selected. This suggests that the interface contained irrelevant DoF to model this operating condition. The improved predictive quality, as shown in the onboard validation, suggests that this subset is a proper interface description. Furthermore, the results are plausible because a similar set of DoF is active for the symmetrically located VPs 1 and 2. They correspond to the left and right VPs of Fig. 20. Their

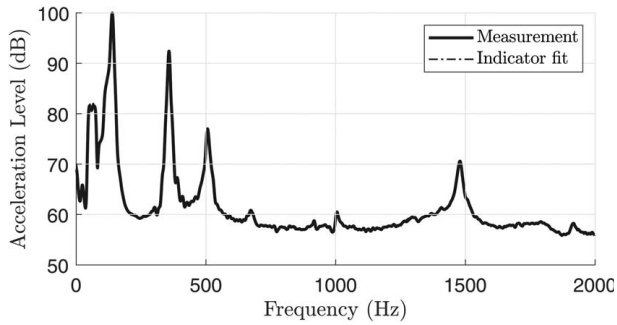

Fig. 21 Indicator validation demonstrating sufficient DoF modeling to describe the measurement

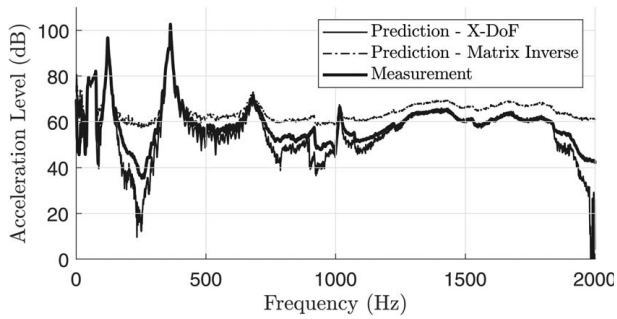

Fig. 22 Onboard validation indicating a reduction of overfitting with X-DoF compared to matrix inverse

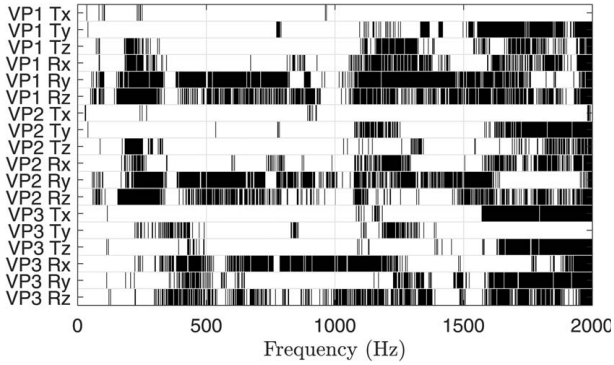

Fig. 23 Subset of active (white) and inactive (black) DoFs that are selected by the X-DoF procedure

Fig. 24 Representative diagram of the active component mounted onto two passive structures

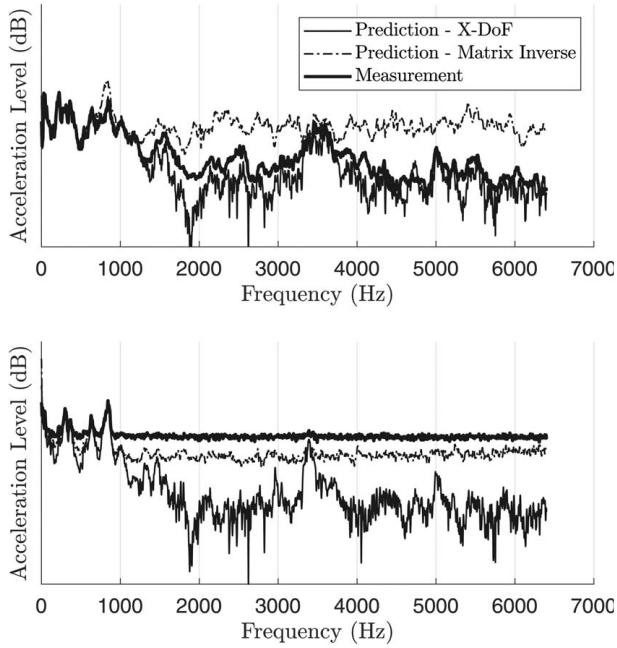

Fig. 26 Onboard validation on two validation sensors indicating that X-DoF reduces overfitting (top) and that overfitting is not always observed (bottom)

moments are mainly active in Rx, corresponding to the stiffest rotational direction of the bushings. As VP3 is located at the bottom, it shows active moments mainly in Ry, corresponding to the stiffest rotational direction of the rubber bushing.

6.2.3 Mechatronic Component. The third test case focuses on transferring blocked forces to another assembly. This component comprises three virtual points with a total of 18 DoF and is mounted in two different assemblies, compare Fig. 24.

To ensure blocked force quality, indicator, onboard, and transfer validation are performed, as in Sec. 3.

Figure 25 shows the validation of the blocked forces at the indicator sensors. For frequencies below 1000 Hz, the fit shows a good match with the measurements. Above 1000 Hz, the fit indicates underfitting, which could be caused by missing blocked force interface DoF or sensor noise. To improve the blocked force characterization above 1000 Hz, one could consider using sensors with a lower noise floor and adding additional blocked force DoF to the interface.

As a next step, the calculated blocked forces are used to predict at unseen validation sensors of the same assembly, see Fig. 26. The figure's first plot (top) indicates overfitting in the predictions with the matrix inverse method. Above a frequency of 500 Hz, using the matrix inverse leads to significant overpredictions. The second plot (bottom) demonstrates that overfitting can not always be observed in onboard validations and underlines the importance of not only relying on the onboard validation to validate the interface description. Up to 1000 Hz, the predictions from X-DoF and the matrix inverse approach do not significantly deviate from the measurements. Above 1000 Hz, the validation sensor cannot validate signals that predict below its noise floor.

The interface description selected by X-DoF for this operating condition is visualized in Fig. 27.

Up to 500 Hz, approximately half of the DoF are active. This indicates that the full matrix inverse model is overfitted in this region. Although overfitting was not observed up to 500 Hz in the onboard validation, a transfer validation should reveal this. As fewer DoFs are active above 1000 Hz, the full model is likely overfitted, which was already observed in the first plot of the onboard validation, see Fig. 26.

As a final step, the blocked forces are transferred and applied to a different test assembly. The transfer predictions are then compared against validation measurements, see Fig. 28. Such a transfer validation is a good test for overfitting because the blocked forces are evaluated on a truly independent dataset.

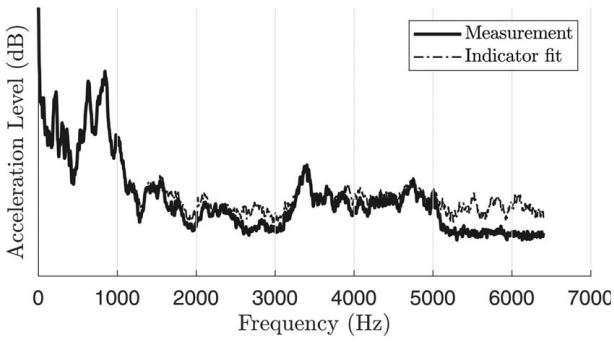

Fig. 25 Indicator validation showing some underfitting of the model above 1000 Hz

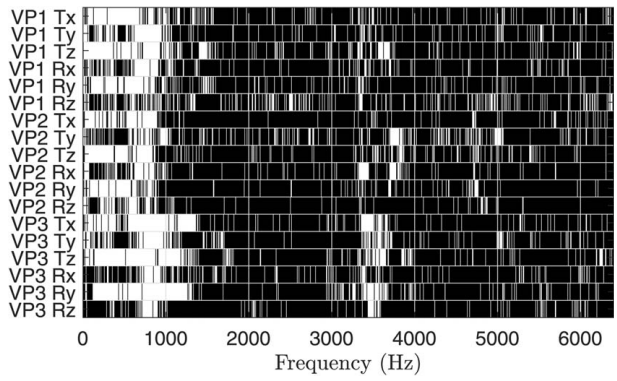

Fig. 27 X-DoF subset of active DoF (white)

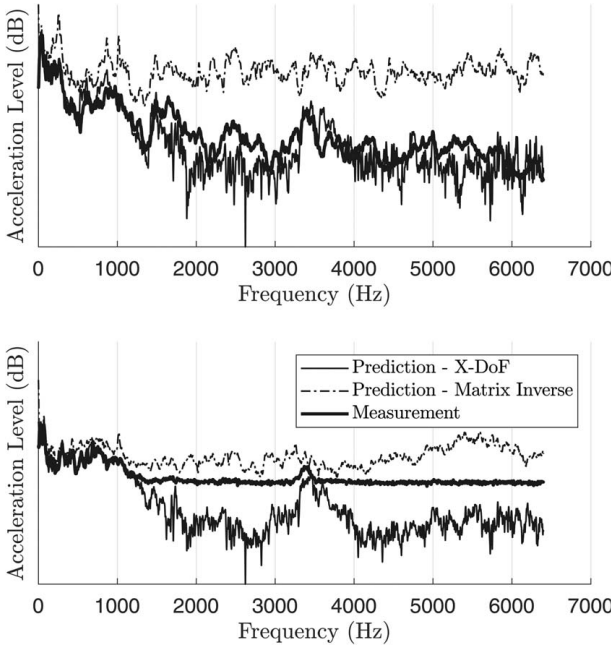

Fig. 28 Transfer validation on two validation sensors showing a reduction of overfitting with X-DoF

The X-DoF transfer prediction is closest to the reference measurement, while the blocked forces from the matrix inverse method yield overpredictions for the entire frequency range. This demonstrates that overfitting was present below 500 Hz, which was not detected in the previous onboard validation because of its insufficient sensitivity to observe overfitting.

Overall, the predictive capabilities of X-DoF are enhanced compared to the matrix inverse method. This can be explained by the matrix inverse approach overfitting noise when irrelevant DoFs are included, which worsens the predictive quality of the blocked forces. The X-DoF procedure shows promising improvements in reducing overfitting, yielding more accurate predictions in regimes where traditional methods might fail.

7 Conclusion

In this work, we have shown that inverse blocked force estimation may suffer from overfitting. This can be caused by sensor noise and the interface description containing too many DoFs. The current techniques to reduce the influence of noise are inadequate because they introduce a bias in the solution. Such a bias can lead to nonphysical blocked force estimates, see Sec. 6.1. This work proposes X-DoF, a procedure to select the best subset of DoF. It does not suffer from the same problems as can be seen in Sec. 5.3. The reason for that is that, by only selecting the relevant subset of DoF, overfitting is reduced. Therefore, the accuracy of the estimated blocked forces increases and their prediction quality significantly improves, as demonstrated in Sec. 6. The necessity for finding the right DoF is not just about prediction accuracy, but also deepening our understanding of the models we create. With the X-DoF procedure, we have found a way to tailor the interface description to the data.

Conflict of Interest

There are no conflicts of interest.

Data Availability Statement

The datasets generated and supporting the findings of this article are obtainable from the corresponding author upon reasonable request.

References

[1] Van der Seijs, M., De Klerk, D., and Rixen, D. J., 2016, "General Framework for Transfer Path Analysis: History, Theory and Classification of Techniques," Mech. Syst. Signal Process., **68**, pp. 217–244.
[2] Elliott, A., and Moorhouse, A. T., 2008, "Characterisation of Structure Borne Sound Sources From Measurement In-situ," J. Acoust. Soc. Am., **123**(5), p. 3176.
[3] De Klerk, D., 2009, "Dynamic Response Characterization of Complex Systems Through Operational Identification and Dynamic Substructuring," Ph.D. thesis, Delft University of Technology, Delft, The Netherlands.
[4] Magrans, F., 2009, "Path Analysis," Proceedings of the NAG/DAGA Conference, Rotterdam, The Netherlands, Mar. 23–26, pp. 768–771.
[5] Van der Seijs, M., Rixen, D., and Klerk, D., 2013, "An Improved Methodology for the Virtual Point Transformation of Measured Frequency Response Functions in Dynamic Substructuring," 4th ECCOMAS Thematic Conference on Computational Methods in Structural Dynamics and Earthquake Engineering, Kos Island, Greece, June 12–14, Vol. 4, pp. 4334–4347.
[6] Haeussler, M., Mueller, T., Pasma, E., Freund, J., Westphal, O., and Voehringer, T., 2020, "Component Tpa: Benefit of Including Rotational Degrees of Freedom and Over-Determination," Proceedings of the International Conference on Noise and Vibration Engineering, Leuven, Belgium, Sept. 7–9, pp. 7–9.
[7] Van der Seijs, M., 2016, "Experimental Dynamic Substructuring: Analysis and Design Strategies for Vehicle Development," Ph.D. thesis, TU Delft, Delft, The Netherlands.
[8] Meggitt, J., Moorhouse, A., and Elliott, A., 2018, "On the Problem of Describing the Coupling Interface Between Sub-structures: An Experimental Test for "Completeness," Dynamics of Coupled Structures, Volume 4: Proceedings of the 36th IMAC, A Conference and Exposition on Structural Dynamics 2018, Orlando, FL, March, Springer, pp. 171–182.
[9] Everitt, B. S., and Skrondal, A., 2010, *The Cambridge Dictionary of Statistics*, Cambridge University Press, Cambridge.
[10] Brunton, S. L., and Kutz, J. N., 2022, *Data-Driven Science and Engineering: Machine Learning, Dynamical Systems, and Control*, 2nd ed., Cambridge University Press, Cambridge.
[11] Haeussler, M., 2021, "Modular Sound & Vibration Engineering by Substructuring," Ph.D. thesis, Technische Universität München, Munich, Germany.
[12] Wernsen, M., 2017, "Observability and Transferability of In-Situ Blocked Force Characterisation," Master's thesis, Delft University of Technology, Delft, The Netherlands.
[13] Hansen, P. C., 1987, "The Truncated SVD as a Method for Regularization," BIT Num. Math., **27**(4), pp. 534–553.
[14] Moorhouse, A., 2003, "Compensation for Discarded Singular Values in Vibro-Acoustic Inverse Methods," J. Sound Vib., **267**(2), pp. 245–252.
[15] Hoerl, A. E., and Kennard, R. W., 1970, "Ridge Regression: Biased Estimation for Nonorthogonal Problems," Technometrics, **12**(1), pp. 55–67.
[16] Pati, Y. C., Rezaiifar, R., and Krishnaprasad, P. S., 1993, "Orthogonal Matching Pursuit: Recursive Function Approximation With Applications to Wavelet Decomposition," Proceedings of 27th Asilomar Conference on Signals, Systems and Computers, Pacific Grove, CA, Nov. 1–3, IEEE, pp. 40–44.
[17] Tibshirani, R., 1996, "Regression Shrinkage and Selection Via the Lasso," J. R. Stat. Soc. Series B: Stat. Methodol., **58**(1), pp. 267–288.
[18] Chen, S., Billings, S. A., and Luo, W., 1989, "Orthogonal Least Squares Methods and Their Application to Non-linear System Identification," Int. J. Control., **50**(5), pp. 1873–1896.
[19] Blumensath, T., and Davies, M. E., 2007, "On the Difference Between Orthogonal Matching Pursuit and Orthogonal Least Squares," University of Southampton, Signal Processing & Control Group, Southampton, UK
[20] Mallows, C. L., 2000, "Some Comments on C_p," Technometrics, **42**(1), pp. 87–94.
[21] Hurvich, C. M., and Tsai, C. -L., 1993, "A Corrected Akaike Information Criterion for Vector Autoregressive Model Selection," J. Seri. Anal., **14**(3), pp. 271–279.
[22] Schwarz, G., 1978, "Estimating the Dimension of a Model," Ann. Stat., **6**(2), pp. 461–464.